Energy 211 (2020) 118678

Contents lists available at ScienceDirect

Energy

journal homepage: www.elsevier.com/locate/energy

Performance enhancement and heat and mass transfer characteristics of direct evaporative building free cooling using corrugated cellulose papers

S.A. Nada [a, b, *], H.F. Elattar [a], M.A. Mahmoud [a], A. Fouda [c]

[a] Department of Mechanical Engineering, Benha Faculty of Engineering, Benha University, Benha, 13511, Qalyubia, Egypt
[b] Egypt-Japan University of Science and Technology, New Borg El-Arab City, 21934, Alexandria, Egypt
[c] Department of Mechanical Power Engineering, Faculty of Engineering, Mansoura University, 35516, El-Mansoura, Egypt

ARTICLE INFO

Article history:
Received 1 April 2020
Received in revised form
18 June 2020
Accepted 19 August 2020
Available online 23 August 2020

Keywords:
Cooling pad
Cooling capacity
Evaporative cooler
Heat and mass transfer
Humidifier effectiveness

ABSTRACT

In hot and dry climatic zones, direct evaporative cooling (DEC) system is used as an economical and efficient alternative to traditional air conditioning systems. The present paper concerns comprehensive experimental investigations and analysis of heat and mass transfer characteristics and thermal performance parameters of a bee-hive construction of corrugated-cellulose papers as a new cooling pad material. The performance parameters used to evaluate the effectiveness of the cooling pad materials are the outlet air temperature and relative humidity, pressure drop, humidifier effectiveness, rate of the evaporated water, sensible cooling capacity, specific cooling capacity (SCC), coefficient of performance (COP), specific water consumption (SWC), and Nusselt and Sherwood numbers. The cooling pad performance was investigated for a wide range of air and water temperatures and flow rates and pad thicknesses. The results show the enhancements of heat and mass transfer coefficients and the performance parameters with rising air temperature and water flow rate to humidifier. High values of the performance parameters ($h_c = 45$ W/m^2 ^{o}C and $h_m = 0.23$ m/s, $\varepsilon_{hum} = 0.85$ and COP = 170) are obtained compared to the traditional pad materials. Experimental correlations for the evaporative cooler performance parameters in terms of air and water temperatures and flow rates pad thicknesses are presented.

1. Introduction

Currently, there is great requests for cooling and air conditioning of buildings especially in hot countries. Conventional cooling and air conditioning systems using vapour compression refrigeration cycle require high demand of electricity supply and this causes problems for government and electric authorities especially in summer peak period. Statistics show that the electric demand of the air conditioning systems in summer season represents about 60% of the electric demands of the domestic sector [1,2]. This high electricity demands causes extra CO_2 emission in the electricity generation process. Moreover, most of the conventional chillers and cooling systems are often run by environmentally hazardous cooling agents. For saving electric power and avoiding environmentally hazardous, using of direct evaporative cooling is becoming preferable solution especially in hot and dry zones. Direct evaporative cooling (DEC) system is one of the most economic and efficient cooling techniques that can be used for buildings cooling especially in hot and dry regions. Cooling process in direct evaporative cooler is attained based on sensible and latent heat transfer between air and sprayed water in the evaporation process. The main components of direct evaporative cooling systems are water tank, water circulating pump and cooling pad section. In the following section, the relevant literature review of the experimental and theoretical research is presented. The review is classified to the following four main topics related to evaporative cooling (i) Potential of using evaporative cooling in different countries and weather conditions and the effects of the operating parameters on its perfromance, (ii) hybrid systems of conventional air conditioning system and evaporative cooling process, (iii) different cooling pad materials used in evaporative cooling, and (vi) research related to heat and mass transfer mechanisms in evaporative cooling. In the following sections, the review of each

* Corresponding author. Benha Faculty of Engineering, Benha University, Benha, 13511, Qalyubia, Egypt.
E-mail address: samehnadar@yahoo.com (S.A. Nada).

https://doi.org/10.1016/j.energy.2020.118678
0360-5442/

Nomenclature

A	pad cross section area, m^2
A_s	contact surface area of evaporative pad material, m^2
c_p	specific heat at constant pressure of moist air, kJ/kg K
D	air thermal diffusion coefficient, m^2/s
g	standard gravitational acceleration, m/s^2
H_P	circulating pump head, m
h	specific enthalpy, kJ/kg
h_c	heat transfer coefficient, W/m^2 °C
h_m	mass transfer coefficient, m/s
L_c	characteristic length of pad, m
Nu	Nusselt number
$\dot{m}$	mass flow rate, kg/s
$\dot{Q}_c$	sensible cooling capacity, kW
q	specific heat losses, kJ/kg
v	mean velocity, m/s
R	gas constant, kJ/kg K
Re	Reynolds number
$\dot{V}$	volume flow rate, m^3/s
V_{pad}	volume of evaporative pad material, m^3
Sh	Sherwood number
$\dot{W}_{fan}$	power consumption of the air fan, kW
$\dot{W}_{pump}$	power consumption of the water pump, kW

Greek symbols

δ	evaporative pad thickness, mm
ΔP	pressure drop of evaporative cooling pad, Pa
Δt	log mean temperature difference, °C
$\Delta \rho$	log mean mass density difference, kg/m^3
ε_{hum}	humidifier effectiveness
ρ	density, kg/m^3
ω	specific humidity ratio of moist air (mass basis), kg_v/kg_a
ξ	surface area per unit volume, m^2/m^3

Subscripts

a	air/dry air
avg	average
$evap$	evaporated
hum	humidifier
in	inlet air flow
out	outlet air flow
v	Water vapour
w	water
wb	wet-bulb

Abbreviations

COP	coefficient of performance
DEC	direct evaporative cooling
SCC	specific cooling capacity, kWh/kg
SWC	specific water consumption, g/h m^2 °C

classification is separately given and discussed in details.

In the last decade, the potential of using evaporative cooling technology has been more utilized in some applications as an alternative to conventional vapour compression cooling systems for different operating conditions. It was reported that DEC systems consume only 25% of the energy consumption of traditional vapour compression air conditioning systems [3,4]. DEC system can reduce the air temperature up to its wet bulb temperature and can be used in air conditioning of different applications in residential and industrial sectors [5–8]. Xu et al. [9] experimentally examined the performance of DEC in a greenhouse of 2304 m^2 area in Shanghai, China. They reported that the obtained results can be used to optimize the energy management of greenhouses in humid conditions. Guan et al. [10] estimated the potential of using DEC in different Australian climates conditions. They reported that in Brisbane increasing the cooling load in the range 30 W/m^2 to 40 W m^{-2}, the required period of cooling increases from 4.06% to 14.89%. Sohani and Sayyaadi [11] modeled and optimized the performance and cost analysis of cellulose cooling pad direct evaporative coolers. A model was developed to estimate payback period, yearly water consumption and the coefficient of performance. Sohani et al. [12] used modeling and statistical tools-artificial neural network, multiple linear regression and genetic programming to obtain pressure drop and the outlet air temperature of direct evaporative coolers. Al-Badri and Al-Waaly [13] theoretically and experimentally investigated the performance of direct evaporative air cooling. The effects of air temperature, air humidity, and water temperature and water and air flow rates on the performance of evaporative cooler were investigated. Somwanshi and Sarkar [14] developed a mathematical model with experimental validation to investigate the performance of an air and water cooler device for the hot and dry climate conditions of Jodhpur, India. They reported that, the cooler worked very well and the highest depression in the temperature of hot water (17.8 °C) was obtained in May. Water temperature depressions of 12.6 °C, 12.9 °C and 8.6 °C were obtained in April, May and June, respectively. Tewari et al. [15,16] conducted studies on ten specified office buildings using direct/indirect evaporative cooler systems in climatic of Jaipur, India during summer season. The results revealed that the evaporative cooler systems can be used at differs temperature and humidity levels than those defined in ASHRAE 55 and ISO 7730 standards and the systems can achieve human comfortable conditions.

Several other researchers presented hybrid systems of conventional air conditioning system and evaporative cooling process to enhance the perfromance of the combined system and reduce the power consumptions [17–20]. Hao et al. [17] presented a mathematical model to optimize the energy consumption of coupling DEC with the condensing unit of air-cooled chiller system (EACC). The hourly weather data for four towns in China were utilized to conduct this study. The results showed a maximum of energy saving in the range is in the range 2.4%–14.0%. Martínez et al. [18] modified the air-cooled condenser unit in split air conditioning system by coupling the unit with various evaporative cooling pad materials of different thicknesses. The purpose of their study was finding the optimum cooling pad thickness that maximizes the COP and energy efficiency of the system. The results indicated that the COP and system cooling capacity increased by 10.6% and 1.8% and compressor power decreased by 11.40% with using cooling pad thickness of 100 mm. Other researches [19–23] were also conducted to propose hybrid systems of evaporative cooling and different conventional air conditioning system for the purpose of cooling and fresh water productions. Different arrangements of the hybrid system were propsed in these studies. The possibility of using solar energy to participate in driving the system was also included in these researches. Effects of operating conditions such as air flow rate, air temperature, flow rate and temperature of feed

water on the cooling effect were also investigated.

A lot of investigations were conducted to propose, study and compare the perfromance of different cooling pad materials used in evaporative cooling. Malli et al. [24] carried out experimental work using a sub sonic wind tunnel to investigate the thermal performance of different types of cellulosic cooling pads. The results revealed that the humidifier effectiveness decreases with increasing frontal air velocity and the evaporated water rate and pressure drop increase with the increase of inlet air velocity. The thermal performance of different new evaporative cooling pad materials such as aspen and khus pads were experimentally analyzed and presented by Jain and Hindoliya [25]. They reported that palash fibers pad efficiency was higher than those of aspen and khus pads by 13.2% and 26.3%, respectively and coconut fibers efficiency was 8.15% greater than that of khus. A novel mathematical model to analyze the effect of the operating conditions on the performance of DEC using porous materials was presented by Sellami et al. [26]. The results displayed that evaporative cooler porous material can achieve the cooling requirements in dry zones. A physical model to investigate the performance of evaporative cooling pad material under different weather conditions of Morocco cities was presented by Laknizi et al. [27]. The system performance was tested and the effects of the pad thickness and air velocity on the system performance were investigated. They reported that water consumption rate and cooling capacity increases and COP decreases with increasing pad thickness and air velocity. Doğramacı et al. [28] experimentally studied the performance of eucalyptus fibre material as an evaporative cooling pad. The results showed that the heights air temperature drop was 11.30 °C with an efficiency of 71% at 0.10 m/s air velocity. Recently Nada et al. [29] showed, based on energy-exergy analysis that corrugated cellulose papers can efficiently be used as cooling pads of evaporative cooling system under the Egypt climates conditions.

The mechanisms and characteristics of heat and mass transfer in the cooling pad section of the evaporative cooling were also investigated in the literature [30–34]. Camargo et al. [30] presented mathematical and experimental study to calculate the heat transfer coefficient from the basic principles of evaporative cooler. The operation principles of the evaporative cooler and the basic mathematical equations of the heat and mass thermal exchanges were developed and presented. The saturation effectiveness was determined from these equations. It was reported that, the effectiveness of heat and mass transfer process in the cooling pads makes the evaporative cooling systems can be used as an efficient and economical alternative to traditional air conditioning systems in hot and dry zones.

Wu et al. [31,32] theoretically analyzed heat and mass transfer in evaporative cooling systems. Heat and mass transfer process between air and water film was theoretically studied. A simple correlation of the cooler efficiency was proposed based on energy balance concept to give the effect of air velocity and cooling pad thickness on the cooling efficiency. Their results displayed also that the optimal air velocity for selecting the face area of cooling pad material for a certain cooling capacity is 2.5 m s^{-1}. They also reported that the direct evaporative cooler may be functional for air conditioning with practical selections of air velocity and cooling pad thickness. Fouda and Melikyan [33] presented a simplified mathematical model to investigate and analyze the performance of direct evaporative coolers. Heat and mass transfer process between air and water was analyzed in the model through the mass and energy conservation equations and their boundary conditions. Latent heat of water during the evaporation process was considered as the heat source of the energy equation and the evaporated water mass was considered as the mass source in the mass conservation equation. The effects of various operating conditions and geometrical parameters on its performance were also investigated. The governing equations of mass and heat transfer in a metallic-compact evaporative cooler using a new design for pad material were solved numerically and presented by Kovačević and Sourbron [34]. A compact direct contact air-water cross flow heat exchanger was considered to cool down the air by water. The model applied energy and mass governing equations for both air and water. Correlations for heat and mass transfer coefficients were considered. The model was solved numerically by Matlab central-finite discretization. The results indicated that the maximum effectiveness is found at evaporative pad cooler thickness of 90 mm and it is affected by air velocity.

Based on the above extensive literature review for hot and dry climatic zones, direct evaporative cooling (DEC) system is used as an economical and efficient alternative to traditional air conditioning systems. Moreover, a lot of studies focused either on the thermal and hydraulic performance or energy saving potential in evaporative cooler system. Very limited studies which directly correlate heat and mass transfer characteristics and the system performance (thermal & hydraulic) in terms of pad thickness, air humidity, air and water temperatures and mass flow rates are available in the literature. Such correlations are important for comparing between pad materials to select the best one. Therefore, it is always needed to propose new more efficient cooling pad materials and evaluate, correlate and compare their performance (thermal & hydraulic) with the existing ones.

In the present study heat and mass transfer characteristics and the thermal-hydraulic performance parameter of bee-hive construction of corrugated cellulose papers cooling pads are experimentally investigated. Comprehensive experimental parametric study is also presented for a wide range of operating conditions and geometrical parameters. The study also aims to predict experimental correlations for heat and mass transfer coefficients and performance parameters in terms of all operating conditions and geometric parameters. The studied cooling pad is made of corrugated cellulose papers in opposite arrangement with a “bee-hive” construction. The manufacturer and supplier of the pad is a Wadi Group company in Egypt, under the trade name of “Tabreed”. The pad has low manufacturing cost, easy and flexible to adjust to any evaporative cooling system and has lower pressure drop.

2. Experimental methodology

2.1. Experimental setup

To investigate the thermal-hydraulic performance of the DEC with the proposed new cooling pad material, an experimental test rig is designed and constructed to test the system at a wide range of operating conditions and geometrical parameters. Different cooling pad sections of different thicknesses were tested under steady-state in a subsonic wind tunnel as shown schematically in Fig. 1. The wind tunnel is a rectangular cross-section of width × height = 390 mm × 335 mm and of 3 m length..

The main components of the experimental test rig are air fan, air heaters, air straightener, water circuit and cooling pad section. Measuring and instrumentation devices are also included in the test rig for measuring air temperatures, air relative humidifies, pressure drop, power consumption, air velocity, water temperature and water mass flow rate. The walls of the wind tunnel are 0.8 mm thick galvanized sheet steel. The wind tunnel walls are thermally insulated by 1- inch thick glass wool insulation to minimize the heat losses from the system and assuring proper heat balance in each section.

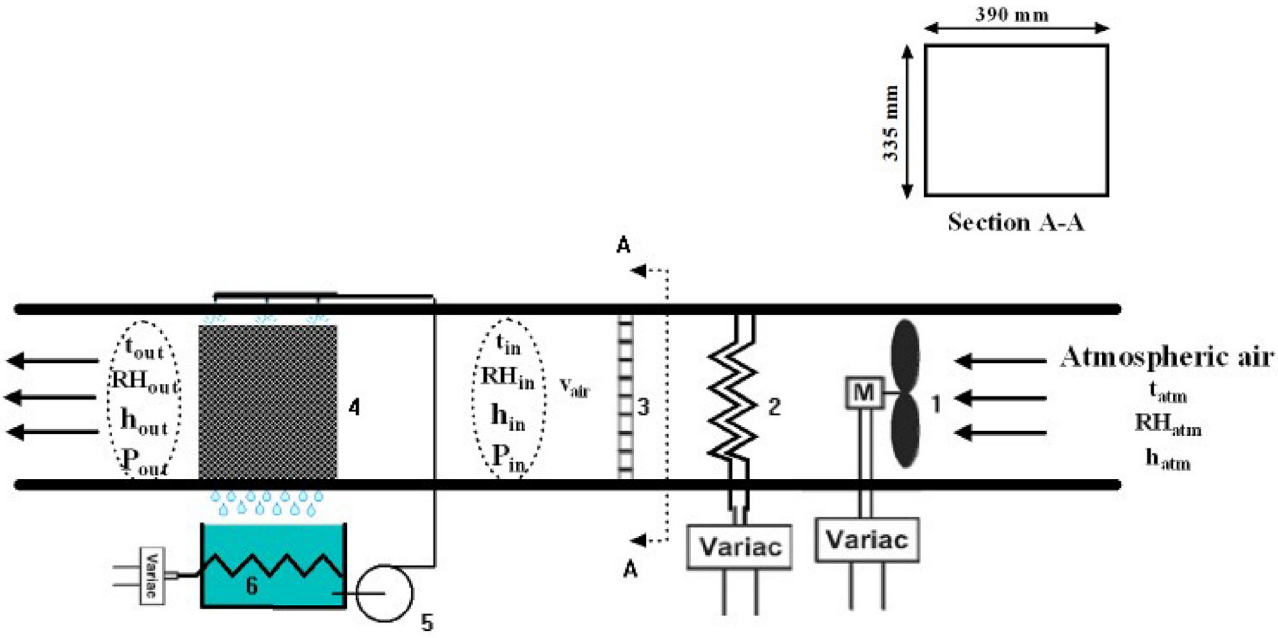

Fig. 1. Schematic diagram of experimental setup: 1. Air fan; 2. Air heaters; 3. Straightener; 4. bee-hive cellulosic pad; 5. Water pump; and 6. water heater.

The test rig contains two loops; air loop and water loop. Air is extracted from atmospheric by air fan (1 Hp, 220 V and 50 HZ). The speed of the fan is controlled by variable transformer (Variac) to control its flow rate. The air is then passed on air heaters (three heaters, 3 kW each) to heat the air to the required temperature. Each heater is made of 3 m long bar steel with 8.5 mm diameter and it is formed in serpentine shape and the heaters are arranged in staggered arrangement in the flow direction to cover the entire cross section area of the tunnel. The temperature of the air is controlled by using a Variac to control the input power to the heater. After that the air is passed through the air mixer and then it flows through an air straightener to obtain on a uniform air velocity and temperature through the duct cross section. Finally, air is passed through the evaporative cooling pad section to humidify and cool it to the required temperature.

In the water loop, a water pump (380-V, 50 Hz, and 10 L/min) is used to pump water from the water tank to a water distributer placed over the evaporative cooling pads section. The tank geometry is 400 × 335 × 390 mm, fabricated from 0.8 mm thick galvanized sheet steel. The water tank contains a water electrical heater (1500 W). The spray water distributer is fabricated from a steel pipe of 1-inch diameter with 13-holes and with spacing of 30 mm and overall length of 500 mm. Water flows downward through the pad section in cross flow arrangement with the air where the air is cooled and humidifying. The temperature of the water in the water tank is controlled by water heater and variable transformer (Variac).

Different instruments and measuring devices are mounted in the test rig to measure air flow rate, water flow rate, air temperatures at the inlet and exit of each section, water temperature at the inlet of the cooling pad section, power of air and water heaters, and pressure drop across the cooling pad section. Two hygrothermometers are placed at upstream and downstream the evaporative cooler, and one more (SH-109) is used to measure the ambient air condition in the Lab. PT100 temperature sensor is coupled with a digital thermometer (model TC4Y) to measure the temperatures at the inlet of the cooling pad. A digital differential pressure manometer (0.5 PSI, HD755) is used to measure the air pressure drop across the cooling pad. Pitot tube anemometer & manometer (HD-350) are used to measures the air velocity and airflow rate in the air duct. The specifications of measuring instruments are given in Table 1.

2.2. Evaporative cooling pad material

A new evaporative cooling pad material is proposed and tested. The cooling pad materials is made of cellulose papers corrugated sheets of 0.7 mm in thickness grouped in the form of a “bee-hive” structure (see Fig. 2). The pad type used is a 45/45 angle. The cooling pad is a product of Wadi Group Company; leader company in the Arab World under the trademark of “Tabreed”. Four cooling pad sections of thickness 35, 70, 105 and 140 mm are tested. The cross section area of the cooling pad section is 0.335 × 0.390 m^2 and the surface area per unit volume (ξ) is 360 m^2/m^3.

2.3. Measurements and procedure

The experiments are performed to study the thermal-hydraulic performance of the DEC system at a wide range of operating conditions and geometric parameters. Eighty two experiments are performed with different cooling pad thicknesses, air velocity, air temperature, humidifier water temperature and flow rate. Measurements in each experiment were recorded at steady state conditions. To achieve steady state condition, the experiment was turned on at least 30−40 min until ensure that the readings of each sensor shouldn’t have significant fluctuations, and then the measurements should be taken. The procedure to conduct the experimental program was as follows.

1. Keeping the air fan flow rate at specific required value.
2. Keeping air temperature at specific required value.
3. Keeping the water flow rate at the specific required value.
4. Keeping the water temperature at the specific required value.
5. Repeating the above steps with different values of the studied operating and geometrical parameters as shown in Table 2.

Table 1
Technical specifications of instrumentations.

Instrumentation	Measured parameters	Resolution	Range	Accuracy
Hygro-thermometer (HTC-1)	Temperature Relative humidity	±0.1 °C ± 1 % RH	−50 to +70 °C 10%–99% RH	±1 °C ± 5 % RH
Hygro-thermometer (SH-109)	Temperature (ambient) Relative humidity (ambient)	±0.1 °C ± 1% RH	−10 to 50 °C indoor −50 to +70 outdoor 20%–99% RH	±1 °C ± 5 % RH
Digital thermometer (PT-100)	Temperature	±0.1 °C	−50 to 400 °C	±1 °C
Digital differential pressure manometer 0.5 PSI (HD755)	Pressure drop (cooling pads)	0.001 Psi	0–0.5 Psi	±0.3%
Pitot tube anemometer & manometer (HD-350)	Measures Air Velocity/Airflow in difficult-to-reach or tight locations	0.01	1–80.00 m/s	±1%

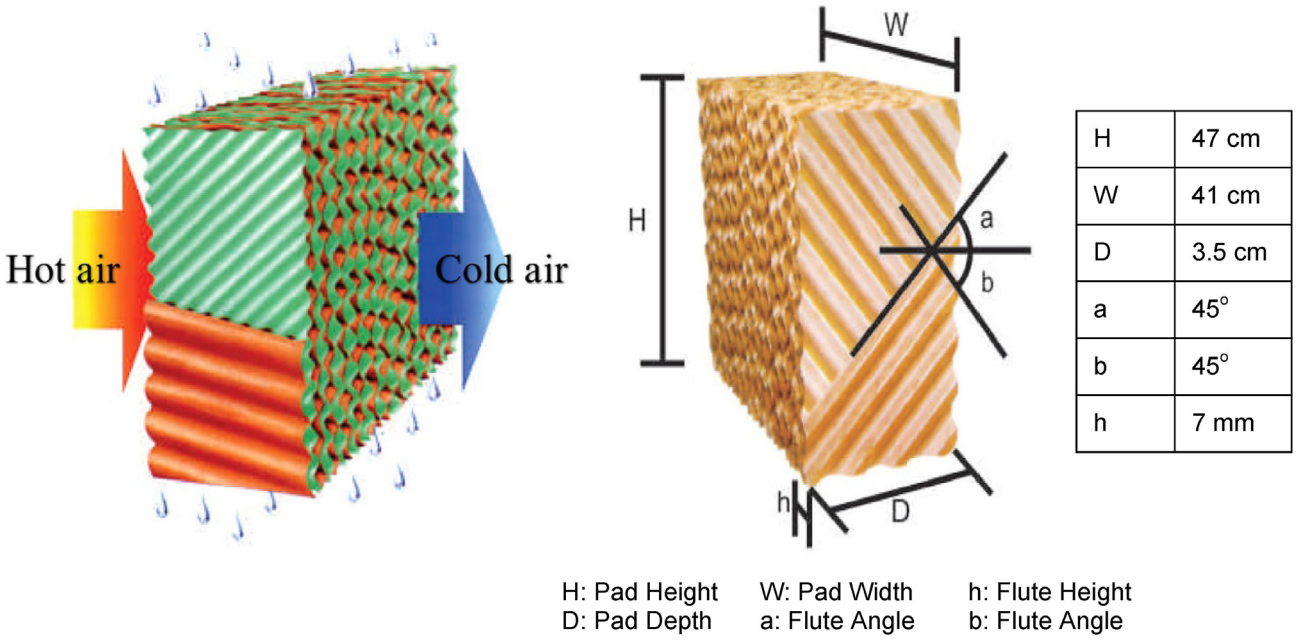

Fig. 2. Configuration and dimensions bee-hive cellulosic pad [27].

2.4. Data reduction and performance analysis

The mass and energy conservation equation of the system sections give.

$$\dot{m}_{a,in} = \dot{m}_{a,out} = \dot{m}_a \tag{1}$$

$$\dot{m}_{w,evap} = \dot{m}_a(\omega_{out} - \omega_{in}) \tag{2}$$

$$\dot{m}_a\, h_{in} + \dot{m}_w\, h_w - \dot{m}_a h_{out} - q = 0 \tag{3}$$

The effectiveness of the humidifier can be calculated by Narayan et al. [35,36].

$$\varepsilon_{hum} = \max\left(\frac{(h_{a,hum,out} - h_{a,hum,in})}{(h_{a,hum,out,ideal} - h_{a,hum,in})}, \frac{(h_{w,hum,in} - h_{w,hum,out})}{(h_{w,hum,in} - h_{w,hum,out,ideal})}\right) \tag{4}$$

$\dot{W}_{fan}$ and $\dot{W}_{pump}$ are the power consumptions for the air fan and water pump and can be calculated as follows [17]:

$$\dot{W}_{fan} = \frac{\dot{V}_{air}\Delta P}{\eta_{fan}} \tag{5}$$

$$\dot{W}_{pump} = \frac{\dot{m}_w\, \rho_w H_P g}{\eta_{pump}} \tag{6}$$

Where η_{fan} and η_{pump} are fan and pump efficiencies, which are taken as 80% [17].

Cooling capacity ($\dot{Q}_c$), specific cooling capacity (SCC) and Specific water consumption (SWC) can be calculated from

$$\dot{Q}_c = \dot{m}_a c_p (t_{in} - t_{out}) \tag{7}$$

Table 2
Studied parameters and their values.

Studied parameter	Value
Frontal air velocity, v_{air}	1, 1.5, 2, 2.5 and 3 m s^{-1}
Air inlet temperature, $t_{db,1}$	30, 35, 40, 45 and 50 °C
Water flow rate, $\dot{m}_w$	0.0465, 0.0952, 0.1176 and 0.1667 kg s^{-1}
Water temperature, t_w	25, 30, 35 and 40 °C
Cooling pad thickness, δ	35, 70, 105 and 140 mm

$$SCC = \frac{\dot{Q}_c}{\dot{m}_{w,evap}} \tag{8}$$

$$SWC = \frac{\dot{m}_{w,evap}}{\Delta T\, A_s} \tag{9}$$

$$\Delta T = \frac{(T_{in} - T_{wb,in}) - (T_{out} - T_{wb,out})}{\ln\left[\frac{(T_{in} - T_{wb,in})}{(T_{out} - T_{wb,out})}\right]} \tag{10}$$

The Reynolds number, convective heat and mass transfer coefficients, Nusselt and Sherwood numbers can be calculated as follows:

$$\mathrm{Re} = \frac{\rho_{avg} v\, L_c}{\mu_{a,avg}} \tag{11}$$

$$h_c = \frac{\dot{Q}_c}{\Delta T\, A_s} \tag{12}$$

$$h_m = \frac{\dot{m}_{w,evap}}{\Delta \rho_v\, A_s} \tag{13}$$

$$Nu = \frac{h_c\, L_c}{k_{a,avg}} \tag{14}$$

$$Sh = \frac{h_m\, L_c}{D_{a,aveg}} \tag{15}$$

where,

$$A_s = V_{pad}\, \xi \tag{16}$$

$$L_c = \frac{V_{pad}}{A_s} \tag{17}$$

$$\Delta\rho_v = \frac{(\rho_{wb,out} - \rho_{v,out}) - (\rho_{wb,in} - \rho_{v,in})}{\ln\left[\frac{(\rho_{wb,out} - \rho_{v,out})}{(\rho_{wb,in} - \rho_{v,in})}\right]} \tag{18}$$

$$D = 2.356\left(\frac{T_{a,avg}}{256}\right)^{1.81} \times 10^{-5} \tag{19}$$

The cooling pad performance was also measured by the coefficient of performance (*COP*), which is the ratio of sensible cooling capacity ($\dot{Q}_c$) to electric power consumption of the fan ($\dot{W}_{fan}$) and water pump ($\dot{W}_{pump}$) [27] and presented as:

$$COP = \frac{\dot{Q}_c}{\dot{W}_{fan} + \dot{W}_{pump}} \tag{20}$$

Performance parameters of the evaporative cooler are determined by solving the above system of equations (Eq. (1) to Eq. (20)) using the Engineering Equation Solver software (EES).

3. Error analysis and experimental work validation

Mofatt [37] and Taylor [38] techniques of obtaining the uncertainty of the experimental results and measured parameters are applied. These uncertainties depend on the measuring instruments errors. Equations from (1) to (20) can be written as follows:

$$y = f(x_1,\ x_2,\ x_3, \ldots, x_n) \tag{21}$$

where y is the calculated variable and $(x_1, x_2, x_3, \ldots, x_n)$ are measured parameters that affect the calculation of y. The uncertainty of y can be obtained from the following equation [37,38]:

$$w_Y = \left[\left(\frac{\partial Y}{\partial X_1} w_1\right)^2 + \left(\frac{\partial Y}{\partial X_2} w_2\right)^2 + \cdots\cdots + \left(\frac{\partial Y}{\partial X_N} w_n\right)^2\right]^{0.5} \tag{22}$$

where w_Y is the total uncertainty, δX_1, δX_2, …δX_n are the uncertainty of the measured variables and $\frac{\partial Y}{\partial X_i}$ is obtained numerically. The errors ranges for the used instruments are given in Table 1. The minimum and maximum value of the uncertainty of experimental

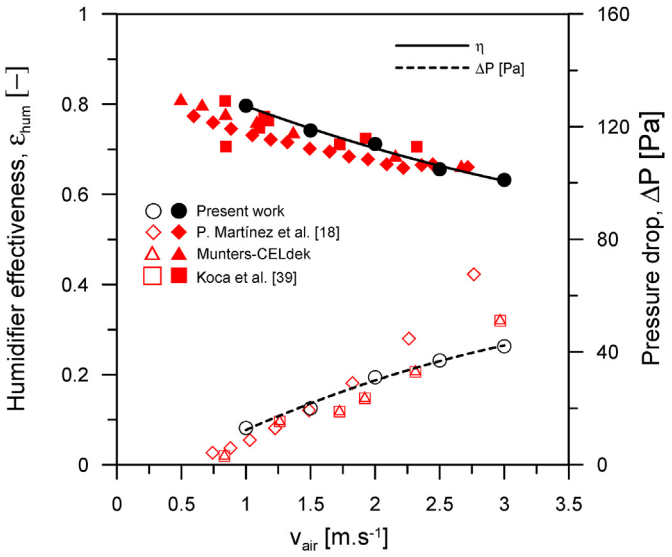

Fig. 3. Validation of the present experimental work with previous studies.

Table 3
Uncertainty of main calculated parameters.

Main Parameters	$\frac{w_{\dot{m}_{w,evap}}}{\dot{m}_{w,evap}}$	$\frac{w_{\dot{Q}_c}}{\dot{Q}_c}$	$\frac{w_{COP}}{COP}$	$\frac{w_{\varepsilon_{hum}}}{\varepsilon_{hum}}$	$\frac{w_{SCC}}{SCC}$	$\frac{w_{SWC}}{SWC}$	$\frac{w_{h_c}}{h_c}$	$\frac{w_{h_m}}{h_m}$	$\frac{w_{Nu}}{Nu}$	$\frac{w_{Sh}}{Sh}$
Uncertainties	±3.5%	±5.2%	±7.4%	±6.8%	±7.4%	±8.2%	±6.7%	±4.7%	±10.6%	±9.3%

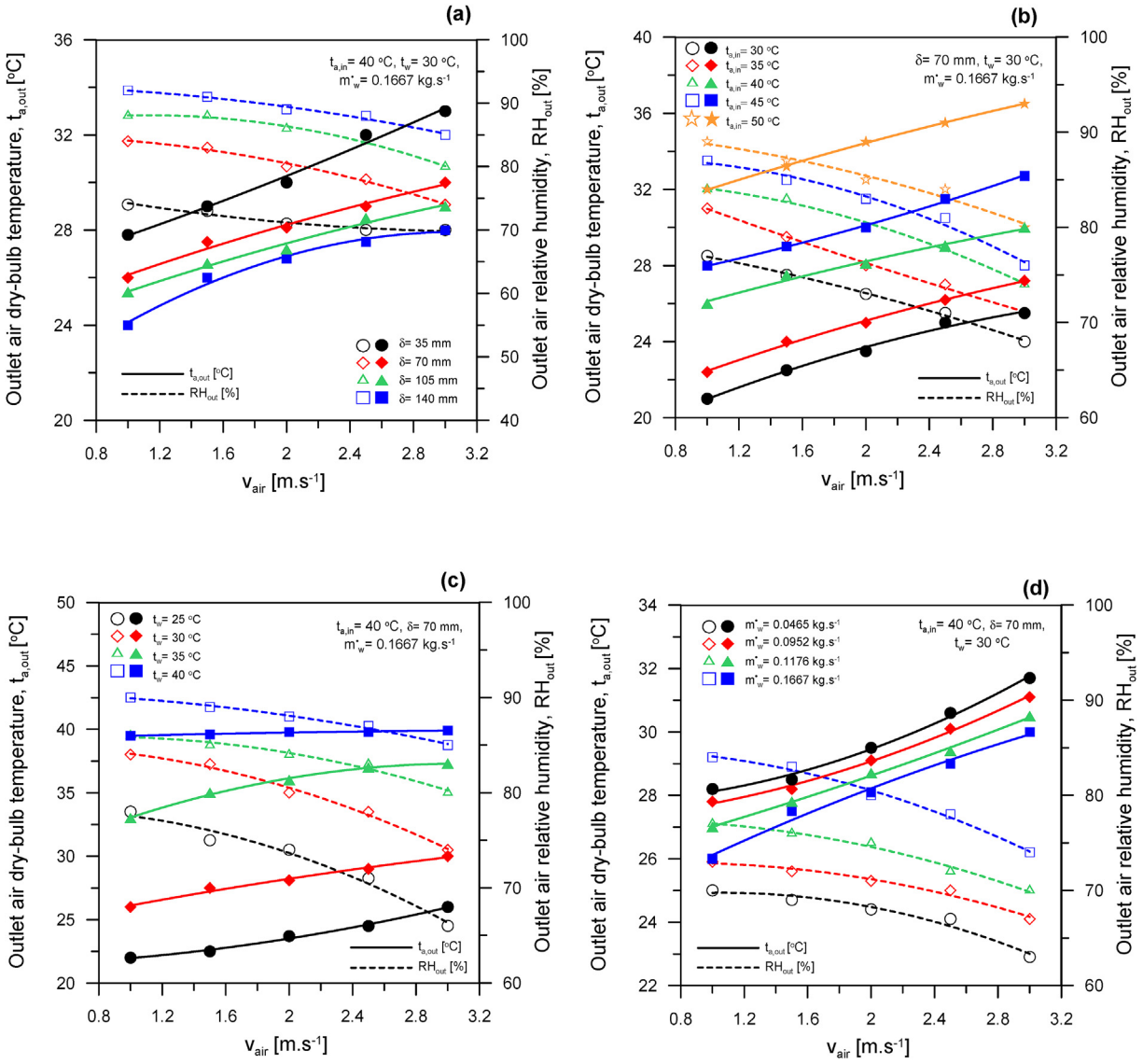

Fig. 4. The effect of pad thickness, air inlet temperature and water temperature & flow rate on outlet air dry bulb temperature and relative humidity.

results and calculated parameters obtained from Eq. (22) are illustrated in Table 3.

To validate the measurements of the present experimental work, numerous tests have been performed on a common cooling pad material (cellulose media, CELdek) by Munters Company. The results of these tests are compared with the available reference data for CELDEK in the literature. The validation tests were conducted by comparing humidifier effectiveness and pressure drop of a cooling pad of thickness 140 mm at a wide range of air velocities. The data was collected from different researchers and compared with data of current experimental tests. As shown in Fig. 3, the current experimental data have the same results obtained by other previous authors. This agreement validate the present experimental work (test rig, experimental procedure, technique of measurements, errors and uncertainty of measurements) to test any other cooling pad materials with confidence in the obtained results and accuracy.

4. Results and discussion

The main objectives of the current work are studying the thermal-hydraulic performance of the new cooling pad material and the effects of operating conditions and geometrical parameters on this performance. Outlet air temperature and relative humidity, pressure drop, humidifier effectiveness, rate of evaporated water, sensible cooling capacity, specific cooling capacity (SCC), coefficient of performance (COP), specific water consumption (SWC), heat and mass transfer coefficients and Nusselt and Sherwood numbers of the new pad material are measured and considered as thermal-hydraulic performance parameters of the cooling pad. The effects of the operating conditions and geometric parameters (air temperature, air and water mass flow rates, water temperature and pad thickness) on these thermal-hydraulic performance parameters are investigated and presented in the following sections. For the assessment and evaluation of the proposed cooling pad materials, the thermal–hydraulic performance of the present direct evaporative cooler are compared with previous data for other selected

pad materials in the literature for the same operating conditions. These comparisons show the prevailing of using the current proposed pad material. Finally, the experimental results are regressed to obtain new experimental correlations for the thermal-hydraulic performance parameters (t_{out}, RH_{out}, ΔP, ε_{hum}, $\dot{m}_{w,evap}$, $\dot{Q}_c$, *SCC*, *COP*, *SWC*, h_c, h_m, *Nu* and *Sh*) of the proposed evaporative cooler pad material in a wide range of operating and geometrical design parameters.

4.1. Mechanism of transport process and heat and mass transfer

Before going to the analysis and discussion of the experimental data it is wort to highlight the underlying mechanisms of the transport process in the evaporation cooling. This well help in investigating and analyze the different trends obtained in the experiments. The concept of simplified models presented in the literature was also cited to better understand the transport process and make the experimental trends more clear.

In the evaporative cooler air is forced to flow through the cooling pad which is contentiously maintained wetted by continues flow of water through it. Normally water flow downwards in the pad medium and the air is in cross flow with it. Due to the difference of water mass concentration in water and air flows, water vapour is transferred from the pad medium to the flowing air causing the air becomes more humid. The process of vapour transfer between the wetted pad medium and the flowing air logically to be dependent on the air properties (air flow rate, air humidity and air temperature) as well as on wetted medium properties (wettability of the medium by water, water flow rate through the wetted medium, the structure of the wetted medium and the water temperature). Evaporation of water in the wetted medium to vapour carried by the flowing air needs heat of evaporation. This latent heat of evaporation is extracted from the air sensible heat causing temperature drop and cooling of air. This heat transfer between the air and the wetted medium depends on the air temperature, air velocity and wetted medium temperature. Thermodynamically, the sensible heat taken form the air is balanced by the heat of evaporation of water. This evaporation of heat is recovered again to the air as a latent heat/latent enthalpy. So, theoretically speaking the enthalpy of the air should be kept

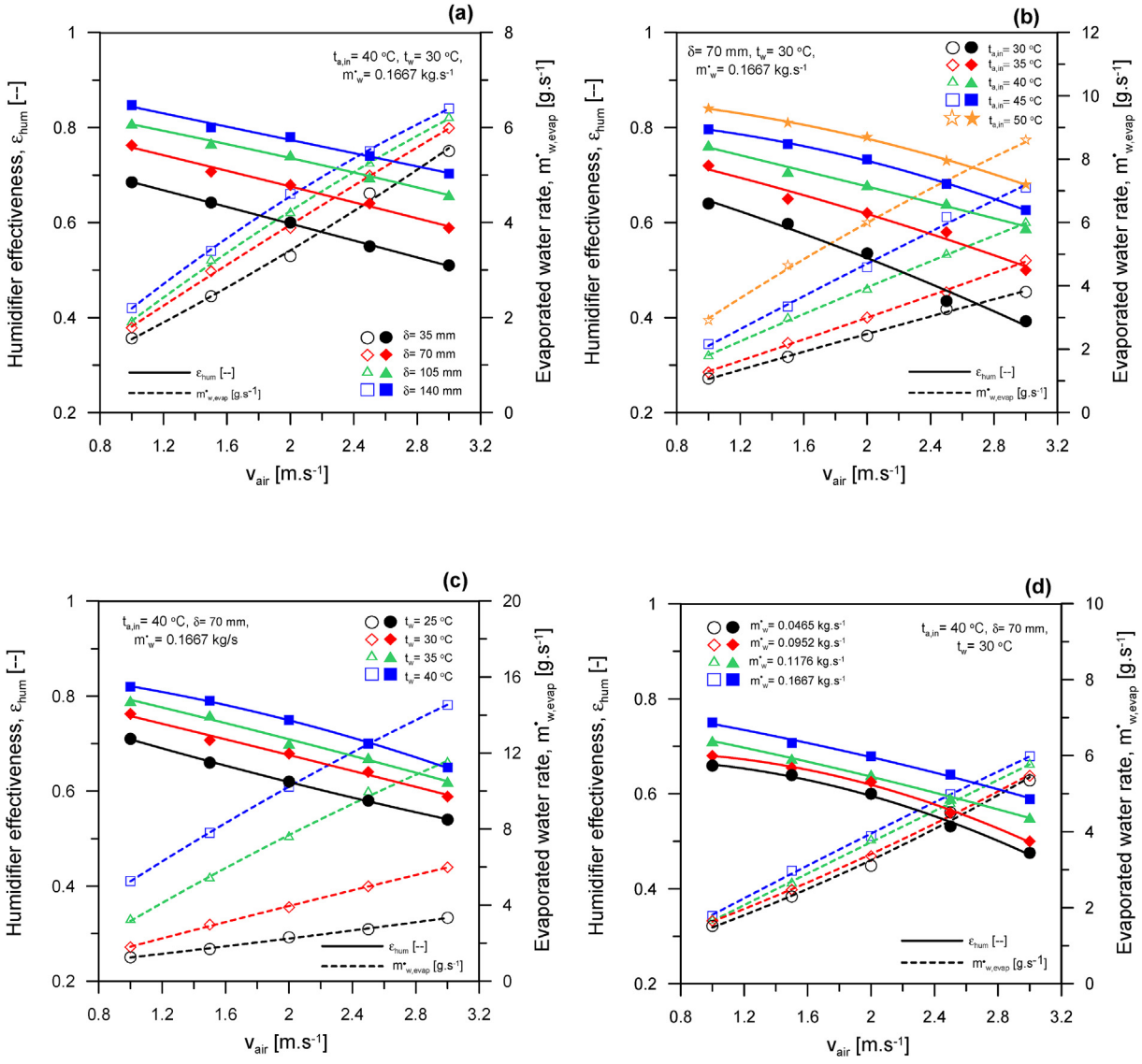

Fig. 5. The effect of pad thickness, air inlet temperature and water temperature & flow rate on humidifier effectiveness and evaporated water rate.

constant through this evaporation process as the drop in the sensible enthalpy equals the increase of the latent enthalpy of air. A deviation may occurs and the enthalpy of air may slightly increase or decrease according to the air and water flow rates and temperatures as well as according to the heat and mass exchanging process in the wetted medium which depends on the medium structure. Finally as a result of this process, the air temperature decreases and the air specific humidity increases as the air passes through the wetted medium. As discussed in this section, the degree of air cooling is expected to depend on a number of factors, including air and water temperatures and flow rate as well as the structure of the wetted medium which controlled the mass and heat transfer during the evaporation process. Accordingly the aim of the present experimental work is to find and correlate the effects of these parameters with using the new proposed wetted medium.

Firstly the traditional cooling pad medium was made from aspen. Currently this old used medium has been replaced by different engineered medium of agriculture products like porous materials and plastic-coated cellulose rigid cooling which is more efficient and has other advantages like good wettability, work as cleaner of the flowing air and the material itself and long life time where the lifetime of these modern cooling pads media can reach to ten times that of the traditional older one. Any new cooling pads media must be experimentally tested to measure and evaluate its effectiveness and perfromance. Also it will be very useful and interesting if we can find correlate the data of the experimental tests to find correlations that predict the perfromance and the heat and mass transfer characteristics of the evaporative cooler using a new cooling pad material.

4.2. Outlet air dry-bulb temperature and air relative humidity

Fig. 4 illustrates effects of cooling pad thickness, air temperature, water temperature, water flow rate and air velocity on outlet air temperature and relative humidity. Fig. 4 displays the increase of t_{out} and the decrease of RH_{out} with the increase of the frontal air velocity. The trend is the same for all operating conditions and geometrical parameters (δ, t_{in}, t_w *and* $\dot{m}_{w,evap}$). This behavior can be attributed to the decrease of contact time between air and cooling pad with the increase of air velocity leading to a lower water

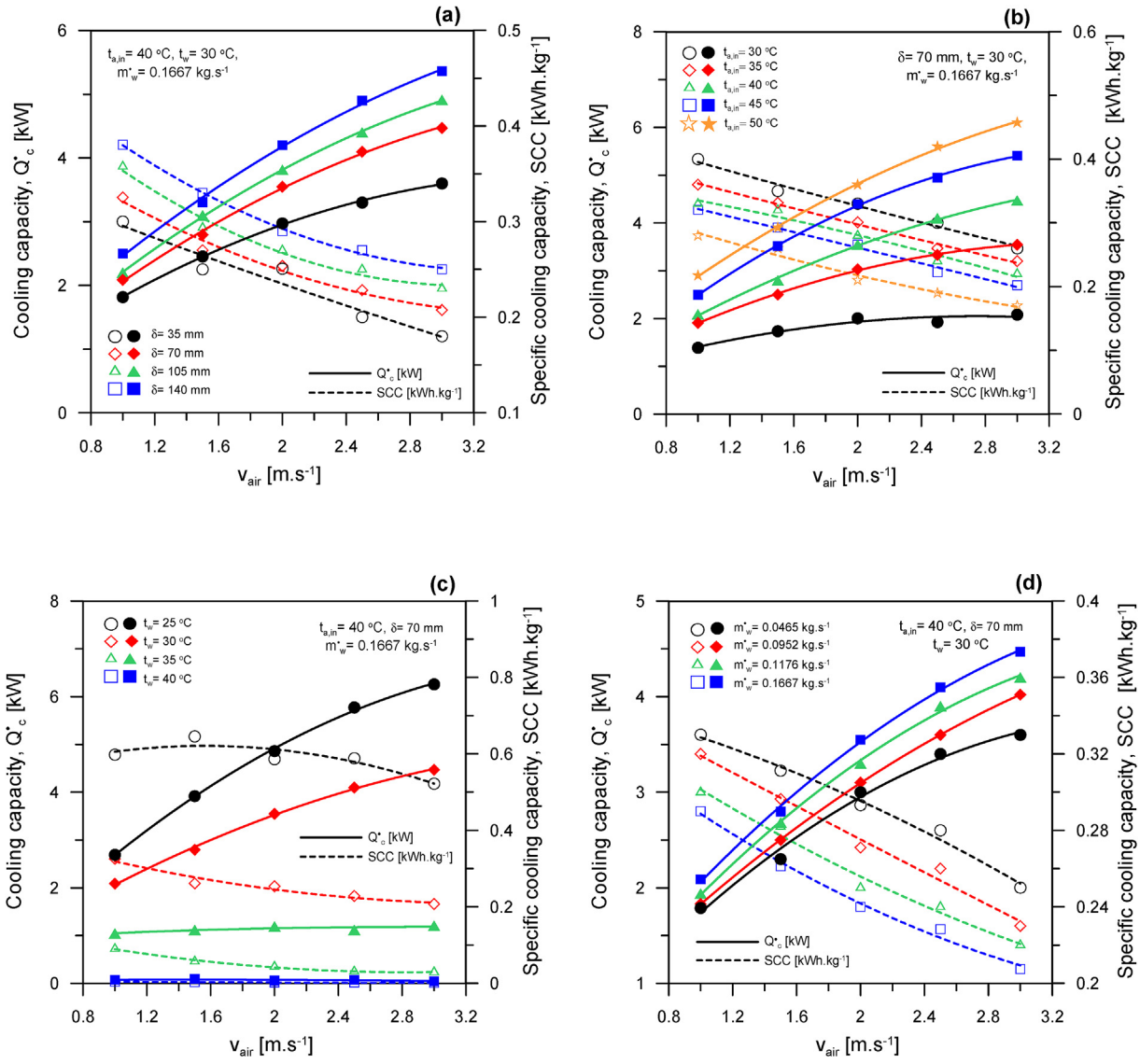

Fig. 6. The effect of pad thickness, air inlet temperature and water temperature & flow rate on cooling capacity and specific cooling capacity.

evaporation rate and lower outlet air relative humidity. This reduction in evaporated water rate causes a decrease in latent and sensible heat transfer between air and the wetted surfaces which lead high outlet air temperature.

The variation of t_{out} and RH_{out} with the pad section thickness for different air velocities at t_{in} = 40.0 °C, t_w = 30.0 °C and $\dot{m}_w$ = 0.167 kg s^{-1} is illustrated in Fig. 4-a. As shown in the figure, the outlet air temperature decreases and air relative humidity increases with increasing the cooling pad thickness. Increasing of the cooling pad thickness increases contact time between air stream and pad surface leading to high evaporation rate and high reduction in outlet air temperature an increase in outlet air relative humidity. The maximum and minimum of (t_{in}-t_{out}) and RH_{out} obtained in this experimental work are 16 °C and 7 °C and 70% and 91% respectively. This means that (t_{in}-t_{out}) and RH_{out} rise by 71% and 21.5% with increasing pad thickness from 35.0 mm to 140.0 mm at 3 m.s^{-1} air velocity.

Effect of air temperature on the temperature and relative humidity of the exit air are demonstrated in Fig. 4-b. As illustrated in Fig. 4-b, the outlet air temperature and air relative humidity increases with increasing air inlet temperature. The possible explanation of that is the increase of the mass transfer between air and the wetted surface of the cooling pad due to the increase of vapour partial pressure in air with the increase of its temperature. Increasing the vapour pressure increases the sensible and latent heat transfer between the air and wetted surface of cooling pad. The maximum temperature differences between inlet and outlet air (t_{in}-t_{out}) at 1 m.s^{-1} air velocity are 9 °C and 18 °C at t_{in} = 30 °C and 50 °C, respectively. Moreover, (t_{in}-t_{out}) and RH_{out} rise by 100% and 16% with rising air temperature from 30 °C to 50 °C, respectively.

Fig. 4-c shows the increase of t_{out} and RH_{out} with the increase of water temperature. This is because of the increase of water evaporation rate which causes an increase in the sensible and latent heat transfer between the air and wetted surface of cooling pad and hence higher t_{out} and RH_{out} can be obtained. Fig. 4-c also shows that (t_{in}-t_{out}) decreased to a minimum value when the temperature of sprayed water was 40 °C and this due to the latent heat transfer became more dominant. The achieved values of (t_{in}-t_{out}) and RH_{out} were 18 and 0.1 °C and 66% and 90% with changing humidifier water temperature from 25 °C to 40 °C, respectively. (t_{in}-t_{out}) and RH_{out} drop and rise by 99% and 28.8% with increasing water temperature from 25.0 °C to 40.0 °C, respectively.

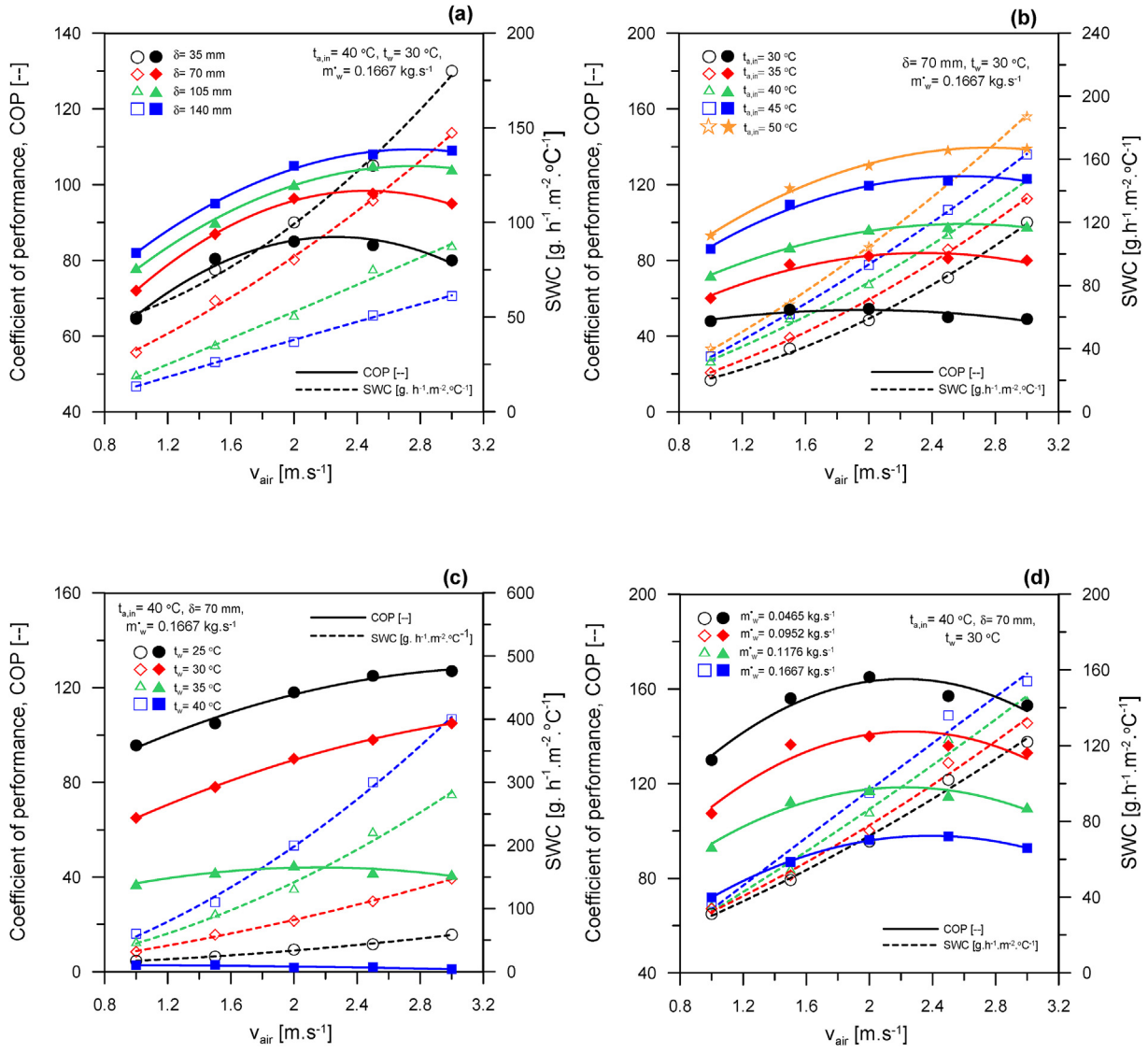

Fig. 7. The effect of pad thickness, air inlet temperature and water temperature & flow rate on coefficient of performance and specific water consumption.

The outlet air temperature and air relative humidity decreases and increases with the increase of the humidifier water flow rate as illustrated in Fig. 4-d. This can be attributed to the increase of the water vapour pressure which causes an increase in the potential of mass transfer causing latent and sensible heat transfers. It's found that the maximum and minimum values of (t_{in}-t_{out}) and RH_{out} are 14 and 9 °C and 84% and 63%, respectively for humidifier water flow rate varies from 0.0465 kg s^{-1} to 0.1667 kg s^{-1}.

The general trends of the effects of the air and water flow rates and temperatures and the thickness of the cooling medium on the outlet air temperature and humidity agree with the trends of the other cooling medium obtained by other investigators [18,24,25,39–42]. A quantitate comparison is needed to compare the perfromance of the current proposed cooling medium (beehive cellulose paper) with other medium. To perform such comparison, the obtained results should be correlated in the form of correlations to be compared with previous correlations of other cooling pads and this will be presented in section 6.

4.3. Humidifier effectiveness and evaporated water rate

The variation of the humidifier effectiveness (ε_{hum}) and evaporated water rate ($\dot{m}_{w,evap}$) with pad thickness, air temperature, water flow rate, water temperature and air velocity are shown in Fig. 5. As displayed in this figure $\varepsilon_{hum}$and $\dot{m}_{w,evap}$ decreases and increases, respectively with increasing air velocity and the trend is the same for all operating conditions. This is due to the decrease in the contact time between air and pad section with the increase of air velocity. The reduction of the contact time leads to the decrease of latent and sensible heat transfer which causes a reduction inε_{hum}. On the other side, $\dot{m}_{w,evap}$ increases with the increase of the inlet air velocity due to the increase of the air mass flow rate which became more dominant than the reduction in latent heat transfer rate.

Fig. 5-a displays the variation of ε_{hum} and $\dot{m}_{w,evap}$ with δ for different air velocities; as shown in the figure ε_{hum} and $\dot{m}_{w,evap}$increase with increasing cooling pad thickness. The increase of the cooling pad thickness causes an increase in the heat and mass

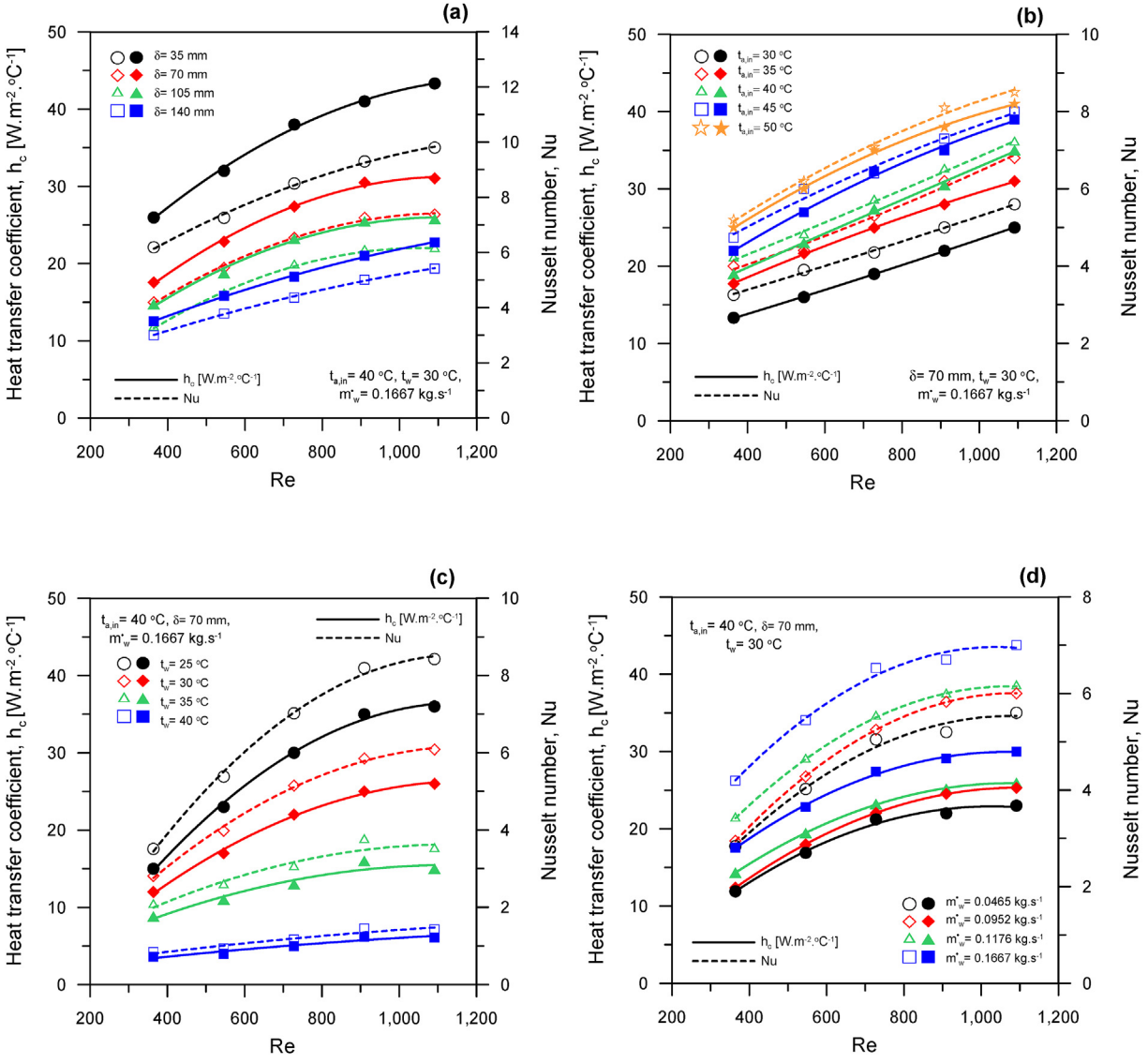

Fig. 8. The effect of pad thickness, air inlet temperature and water temperature & flow rate on heat transfer coefficient and Nusselt number.

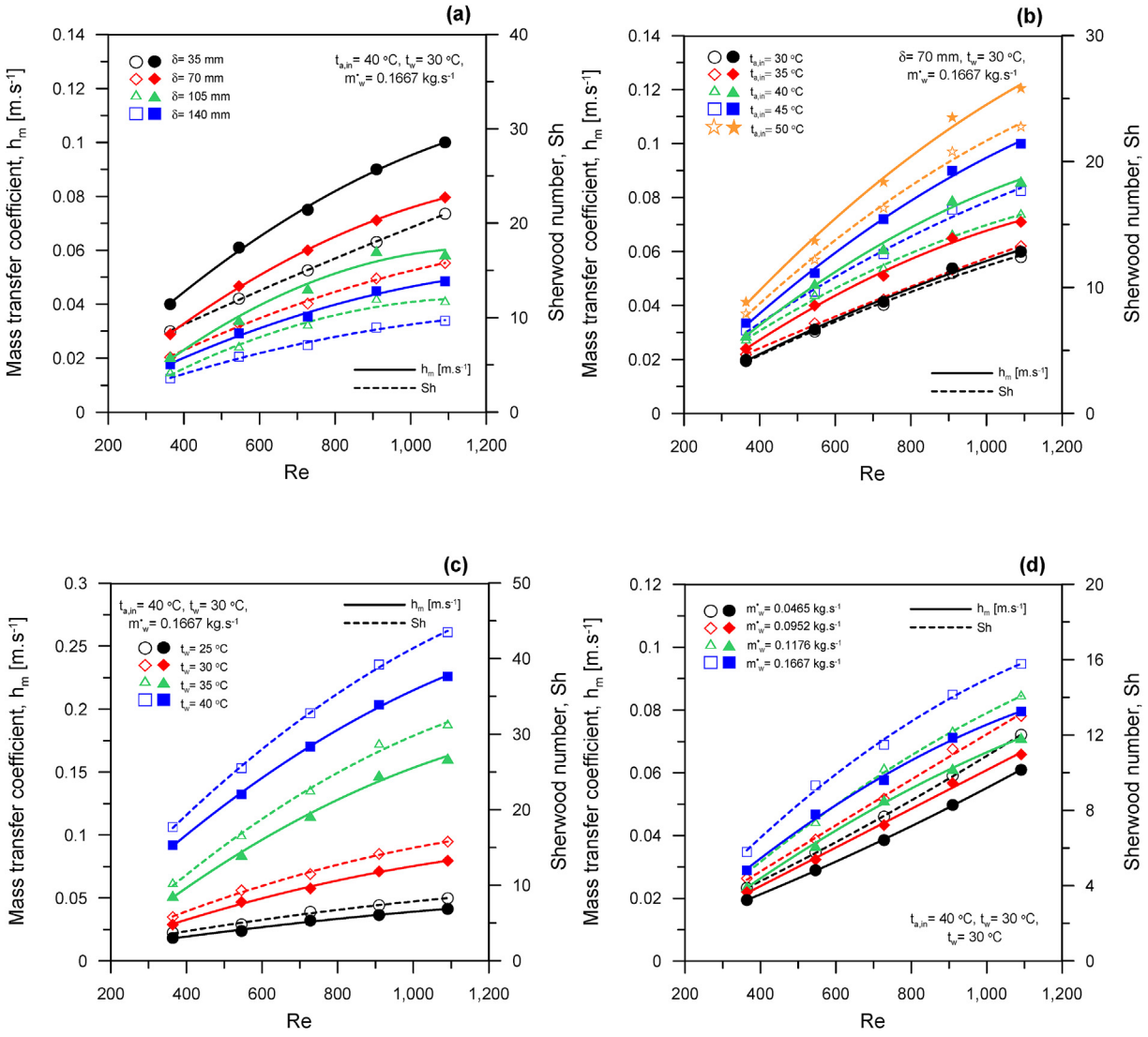

Fig. 9. The effect of pad thickness, air inlet temperature and water temperature & flow rate on mass transfer coefficient and Sherwood number.

transfer rate between air and the pad surface leading to higher evaporation rate and humidifier effectiveness. The highest and lowest ε_{hum} and $\dot{m}_{w,evap}$ that can be attained are 0.85 & 0.51 and 6.5 g/s & 1.5 g s^{-1} at δ of 140 mm & 35 mm, respectively. Moreover, ε_{hum} and $\dot{m}_{w,evap}$increase by 37.8% and 18.2% by the increase of δ from 35.0 mm to 140.0 mm at 3 m.s^{-1} frontal air velocity.

Fig. 5-b shows that increasing the inlet air temperature causes the increasing of ε_{hum} and $\dot{m}_{w,evap}$. This is because of the increase of heat and mass transfer with the increase of the air inlet temperature. As shown in Fig. 5-b, ε_{hum} and $\dot{m}_{w,evap}$increase by 61% and 79%, respectively with increasing the inlet air temperature from 30 °C to 50 °C at 3 m s^{-1} frontal air velocity.

Fig. 5-c and 5-d show the increase of ε_{hum} and $\dot{m}_{w,evap}$with increasing t_w *and* $\dot{m}_w$. This is due to the increase of evaporation rate with the increase of t_w *and* $\dot{m}_w$ and this leads to the increase of the latent and sensible heat transfer rates. As presented in Fig. 5-c, ε_{hum} and $\dot{m}_{w,evap}$rise by 20.3% and 336%, respectively with rising t_w from 25 °C to 40 °C at 3 m s^{-1} frontal air velocity. Moreover, ε_{hum} and $\dot{m}_{w,evap}$ increase by 25.1% and 12.0%, respectively with increasing $\dot{m}_w$ from 0.0465 kg s^{-1} to 0.167 kg s^{-1}, respectively.

The trends of the variation of the humidifier effectiveness with air and water flow rates and temperatures and the thickness of the cooling medium agrees with the trends obtained by previous investigators for other medium [24,25,27,40–42]. A quantitate comparison shows that the humidifier effectiveness of the propsed cooling medium (bee-hive cellulose paper) is always higher than those obtained by the other previous investigators for other cooling medium. Detailed quantities comparison is given in section 6.

4.4. Cooling capacity and specific cooling capacity

The variation of the cooling capacity ($Q_{\cdot c}$) and specific cooling capacity (*SCC*) with v_{air}, δ, t_{in}, t_w and $\dot{m}_w$ are illustrated in Fig. 6. As shown in this figure, $Q_{\cdot c}$ and *SCC* increases and decreases, respectively with increasing v_{air} for all studied parameters. This is attributed to the increase in air mass flow rate which is more dominant than the decrease of air temperature difference (t_{in}-t_{out}) and contact time between air and cooling pad as a result of the increase of air velocity. The decrease of *SCC* is due to the increase of $\dot{m}_{w,evap}$which has more effect on *SCC* than the effect of increase of $Q_{\cdot c}$ with v_{air}.

Table 4
Experimental correlations prediction and their errors.

Experimental correlations	Error range
$\Delta P[Pa] = 0.045 \left(\frac{t_{a,in}}{t_{a,Ref}}\right)^{0.516} \left(\frac{t_w}{t_{w,Ref}}\right)^{-0.695} \left(\frac{\dot{m}_w}{\dot{m}_{w,Ref}}\right)^{0.228} \left(\frac{\delta}{\delta_{Ref}}\right)^{0.626} Re^{1.044} Pr^{0.33}$	Predicts 80% of the experimental results within error ±25%.
$t_{a,out}[^oC] = 21.2 \left(\frac{t_{a,in}}{t_{a,Ref}}\right)^{0.752} \left(\frac{t_w}{t_{w,Ref}}\right)^{1.275} \left(\frac{\dot{m}_w}{\dot{m}_{w,Ref}}\right)^{-0.0313} \left(\frac{\delta}{\delta_{Ref}}\right)^{-0.099} Re^{0.133} Pr^{0.33}$	Predicts 93% of the experimental results within error ±12%.
$RH_{out}[\%] = 200.1 \left(\frac{t_{a,in}}{t_{a,Ref}}\right)^{0.298} \left(\frac{t_w}{t_{w,Ref}}\right)^{0.405} \left(\frac{\dot{m}_w}{\dot{m}_{w,Ref}}\right)^{0.145} \left(\frac{\delta}{\delta_{Ref}}\right)^{0.16} Re^{-0.088} Pr^{0.33}$	Predicts 90% of the experimental results within error ±18%.
$\varepsilon_{hum} = 4.33 \left(\frac{t_{a,in}}{t_{a,Ref}}\right)^{0.756} \left(\frac{t_w}{t_{w,Ref}}\right)^{1.682} \left(\frac{\dot{m}_w}{\dot{m}_{w,Ref}}\right)^{0.065} \left(\frac{\delta}{\delta_{Ref}}\right)^{0.24} Re^{-0.153} Pr^{0.33}$	Predicts 85% of the experimental results within error ±22%.
$\dot{m}_{w,evp}[g/s] = 0.028 \left(\frac{t_{a,in}}{t_{a,Ref}}\right)^{2.26} \left(\frac{t_w}{t_{w,Ref}}\right)^{4.48} \left(\frac{\dot{m}_w}{\dot{m}_{w,Ref}}\right)^{0.071} \left(\frac{\delta}{\delta_{Ref}}\right)^{0.186} Re^{1.057} Pr^{0.33}$	Predicts 87% of the experimental results within error ±19%.
$\dot{Q}_c[kW] = 0.04 \left(\frac{t_{a,in}}{t_{a,Ref}}\right)^{1.795} \left(\frac{t_w}{t_{w,Ref}}\right)^{-2.613} \left(\frac{\dot{m}_w}{\dot{m}_{w,Ref}}\right)^{0.08} \left(\frac{\delta}{\delta_{Ref}}\right)^{0.317} Re^{0.664} Pr^{0.33}$	Predicts 83% of the experimental results within error ±23%.
$SCC\ [kWh/kg] = 0.46 \left(\frac{t_{a,in}}{t_{a,Ref}}\right)^{-0.776} \left(\frac{t_w}{t_{w,Ref}}\right)^{-4.59} \left(\frac{\dot{m}_w}{\dot{m}_{w,Ref}}\right)^{-0.093} \left(\frac{\delta}{\delta_{Ref}}\right)^{0.199} Re^{-0.281} Pr^{0.33}$	Predicts 79% of the experimental results within error ±18%.
$COP\ [-] = 22.22 \left(\frac{t_{a,in}}{t_{a,Ref}}\right)^{1.66} \left(\frac{t_w}{t_{w,Ref}}\right)^{-1.952} \left(\frac{\dot{m}_w}{\dot{m}_{w,Ref}}\right)^{-0.467} \left(\frac{\delta}{\delta_{Ref}}\right)^{0.185} Re^{0.216} Pr^{0.33}$	Predicts 85% of the experimental results within error ±20%.
$SWC[g/h\ m^{2o}C] = 0.018 \left(\frac{t_{a,in}}{t_{a,Ref}}\right)^{1.114} \left(\frac{t_w}{t_{w,Ref}}\right)^{4.427} \left(\frac{\dot{m}_w}{\dot{m}_{w,Ref}}\right)^{0.033} \left(\frac{\delta}{\delta_{Ref}}\right)^{-0.543} Re^{1.456} Pr^{0.33}$	Predicts 86% of the experimental results within error ±16%.
$Nu = 0.112 \left(\frac{t_{a,in}}{t_{a,Ref}}\right)^{0.9} \left(\frac{t_w}{t_{w,Ref}}\right)^{-1.487} \left(\frac{\dot{m}_w}{\dot{m}_{w,Ref}}\right)^{0.186} \left(\frac{\delta}{\delta_{Ref}}\right)^{-0.48} Re^{0.527} Pr^{0.33}$	Predicts 92% of the experimental results within error ±20%.
$Sh = 0.097 \left(\frac{t_{a,in}}{t_{a,Ref}}\right)^{1.374} \left(\frac{t_w}{t_{w,Ref}}\right)^{4.34} \left(\frac{\dot{m}_w}{\dot{m}_{w,Ref}}\right)^{0.304} \left(\frac{\delta}{\delta_{Ref}}\right)^{-0.474} Re^{0.922} Sc^{0.33}$	Predicts 95% of the experimental results within error ±18%.

Fig. 6-a and 6-b shows the increase of $\dot{Q}_c$ with increasing the thickness of cooling pad and air temperature, while *SCC* increases and decrease with the increase of cooling pad thickness and inlet air temperature, respectively. These can be attributed to the increase of the air temperature drop and evaporate water rate with the increase of the pad thickness. As revealed in Fig. 6-a, the maximum and minimum values of $\dot{Q}_c$ and *SCC* are 5.5 kW & 1.82 kW and 0.385 kWh.kg^{-1} & 0.18 kWh.kg^{-1}, respectively. Furthermore, $\dot{Q}_c$ and *SCC* increase by 48.8% and 38.8% with rising δ from 35 mm to 140 mm at 3 m s^{-1} frontal air velocity. Fig. 6-b demonstrates that the maximum and minimum values of $\dot{Q}_c$ and *SCC* that can be obtained are 6.1 kW & 1.91 kW and 0.36 kWh.kg^{-1} & 0.17 kWh.kg^{-1}, respectively and $\dot{Q}_c$ and *SCC* increase and decrease by 193.2% and 52.2% with the increase of air temperature from 30.0 °C to 50.0 °C, respectively at 3 m s^{-1} air velocity.

The effects of humidifier water temperature and flow rate on $\dot{Q}_c$ and *SCC* are shown in Fig. 6-c and 6-d. As illustrated in these figures $\dot{Q}_c$ decreases and increases with increasing of t_w *and* $\dot{m}_w$, respectively. This can be attributed to the decrease and increase of the air temperature drop (t_{in}-t_{out}) with the increase of t_w and$\dot{m}_{w,evap}$, respectively. Fig. 6-c and 6-d also shows that *SCC* decreases with increasing of t_w *and*$\dot{m}_{w,evap}$, and this because of the increase of water evaporation rate is bigger than the increase of $\dot{Q}_c$ with rising of t_w *and*$\dot{m}_{w,evap}$.

4.5. Coefficient of performance and specific water consumption

The coefficient of performance (COP) is defined as the ratio of cooling capacity to the electric power consumption of air fan and water pump. The specific water consumption (SWC) is one of the measuring performance parameters of the evaporative cooling pads material. SWC is defined as the ratio of evaporated water rate per unit surfaces area of pad material to the mean temperature difference. Fig. 7 displays effects of air velocity, pad thickness, air temperature, water temperature and water flow rate on COP and SWC. As can be seen, COP increases by increasing air velocity up to 2.2 m s^{-1} and then COP decreases with the increase of the velocity. By rising the air velocity up to 2.2 m s^{-1}, the air flow rate and pressure drops through cooling pad increase and this increases the fan power consumption but the increase in the cooling capacity is still dominant and vice versa at frontal air velocity >2.2 m s^{-1}. The highest COP was found to be 170 at t_{in} = 40 °C, δ = 70 mm, t_w = 30 °C and v_{air} = 2.2 m s^{-1}.

As illustrated in Fig. 7-a and 7-b, COP increases with increasing the cooling pad thickness and inlet air temperature. This is because of the increase of $\dot{Q}_c$ is superior to the increase of air fan power consumption. Fig. 7-c and 7-d show that COP decreases with the increase of water temperature and flow rate; this is due to the increase of fan and pump power consumptions with a rate greater than the rate of the increase of the cooling capacity.

Fig. 7-a, 7-b, 7-c and 7-d, shows that SWC increases with increasing t_{in}, t_w *and* $\dot{m}_{w,evap}$ and decreases with the increase of δ. This can be attributed to the nature of the relation between the cooling capacity and power consumption of air fan and water pump that was discussed in the previous sections. The highest and lowest COP was found to be 105 and 85 for δ of 140 mm and 35 mm, respectively at 2 m/s air velocity. COP improves by 23.5% with rising δ from 35 mm to 140 mm. Moreover, the optimal value of COP (see Fig. 7-d) is 170 at water flow rate and air velocity of 0.0465 kg s^{-1} and 2 m.s^{-1}, respectively. The COP improves by 71.3% with decreasing $\dot{m}_{w,evap}$from 0.167 kg s^{-1} to 0.046 kg s^{-1}.

4.6. Heat and mass transfer coefficients

The most important objective and novelty of the present work is to add new operating and geometrical design parameters to the

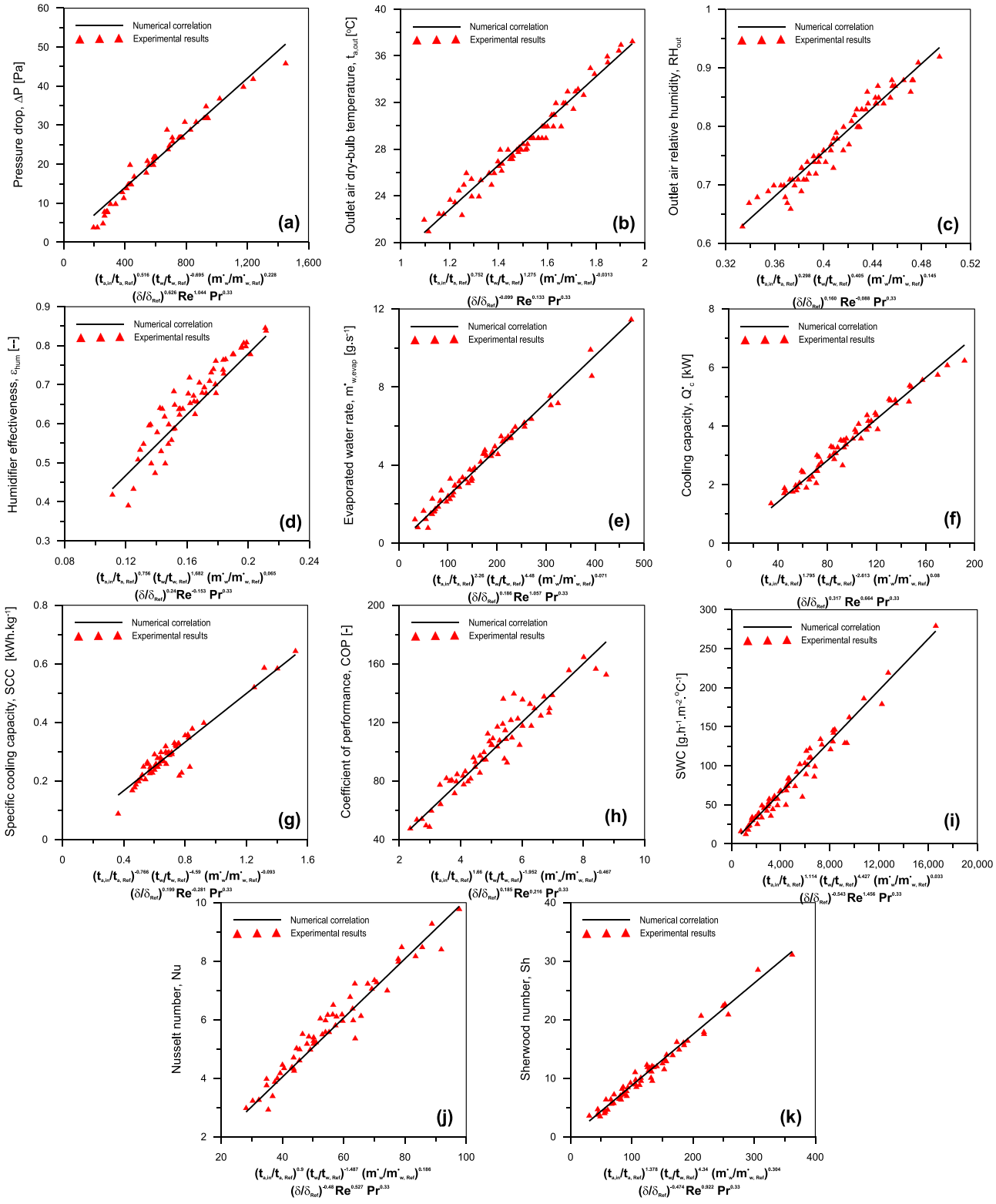

Fig. 10. Experimental correlations prediction of direct evaporative pad cooling system.

existing (traditional) correlations of *Nu* and *Sh* to present new, comprehensive, accurate and useful correlations that can be used in the evaporative cooler design. Figs. 8 and 9 show the increase of heat-transfer coefficient, Nusselt number, mass-transfer coefficient and Sherwood number by increasing Reynolds number. The heat transfer coefficient and Nusselt number are directly proportional to the cooling capacity and inversely proportional to the temperature difference between inlet and outlet air. The mass transfer coefficient and Sherwood number are directly proportional to the rate of evaporated water and inversely proportional to the densities

Table 5
Comparisons with previous types of evaporative pads.

Refs.	Material type	V_{air} (m.s^{-1})	δ (mm)	ΔP (Pa)	$\dot{m}_{w,evap}$(L.min^{-1})	ε_{hum}	*COP*	h_c (W.m^{-2}k^{-1})	h_m (m.s^{-1})
Jain & Hindoliya [25]	Palash Fibre	0.91–1.4	–	29–39	–	0.81–0.84	–	2.615–8.980	0.021–0.046
Laknizi et al. [27]	Cellulosic pad cooling	0.5–3	100–300	5–200	–	0.71–0.96	18–175	–	–
Martínez et al. [18]	Plastic mesh	0.2–2.7	80–250	0.2–17	0.006–0.108	0.35–80	–	–	–
Malli et al. [24]	cellulosic pads (7090)	1.8–4	75–150	15–75	0.06–0.13	0.57–0.85	–	–	–
Present work	Cellulose (bee-hive)	1–3	35–140	4–46	0.18–0.9	0.38–0.85	42–170	9–45	0.018–0.23

Table 6
Comparisons with previous experimental correlations.

Refs.	Material type	Experimental correlations.
Dowdy and Karabash [40]	Cellulosic pad cooling	$Nu = 0.10\left(\frac{l_e}{\delta}\right)^{0.12} \mathrm{Re}^{0.8}\mathrm{Pr}^{\frac{1}{3}}$, *where*, $l_e = \frac{1}{\xi}$
Liao and Chiu [41]	Coarse fabric PVC sponge mesh	$Nu = 4\times10^{-4}\left(\frac{l_e}{\delta}\right)^{0.45} \mathrm{Re}^{0.89}\mathrm{Pr}^{\frac{1}{3}}\left(\frac{\mathrm{Pr}}{\mathrm{Pr}_s}\right)^{\frac{1}{4}}$
		$Sh = 3\times10^{-4}\left(\frac{l_e}{\delta}\right)^{0.45} \mathrm{Re}^{0.89}\mathrm{Pr}^{\frac{1}{3}}\left(\frac{Sc}{Sc_s}\right)^{\frac{1}{4}}$
	Fine fabric PVC sponge mesh	$Nu = 4.7\times10^{-3}\left(\frac{l_e}{\delta}\right)^{0.19} \mathrm{Re}^{0.43}\mathrm{Pr}^{\frac{1}{3}}\left(\frac{\mathrm{Pr}}{\mathrm{Pr}_s}\right)^{\frac{1}{4}}$
		$Sh = 1.7\times10^{-3}\left(\frac{l_e}{\delta}\right)^{0.19} \mathrm{Re}^{0.43}\mathrm{Pr}^{\frac{1}{3}}\left(\frac{Sc}{Sc_s}\right)^{\frac{1}{4}}$
He et al. [42]	Cellulose media	$\Delta P[Pa] = 0.124\left(\frac{l_e}{\delta}\right)^{-1.038}\left(1+1825\frac{\dot{V}_w}{\dot{V}_a}\right)\frac{\rho_a v_a^2}{2}$
		$Nu = 0.192\left(\frac{l_e}{\delta}\right)^{-0.191}\left(\frac{t_{a,in}-t_{wb}}{t_w}\right)^{-0.03}\mathrm{Re}^{0.682}\mathrm{Pr}^{\frac{1}{3}}$
	PVC media	$\Delta P[Pa] = 0.566\left(\frac{l_e}{\delta}\right)^{-0.664}\left(1+3191\frac{\dot{V}_w}{\dot{V}_a}\right)\frac{\rho_a v_a^2}{2}$
		$Nu = 0.210\left(\frac{l_e}{\delta}\right)^{-1.113}\left(\frac{t_{a,in}-t_{wb}}{t_w}\right)^{-0.3372}\mathrm{Re}^{0.223}\mathrm{Pr}^{\frac{1}{3}}$
	A combined correlation for Cellulose and PVC media	$\Delta P[Pa] = 0.219\left(\frac{l_e}{\delta}\right)^{-0.910}\left(1+2031\frac{\dot{V}_w}{\dot{V}_a}\right)\frac{\rho_a v_a^2}{2}$
		$Nu = 0.048\left(\frac{l_e}{\delta}\right)^{-0.890}\left(\frac{t_{a,in}-t_{wb}}{t_w}\right)^{0.1}\mathrm{Re}^{0.515}\mathrm{Pr}^{\frac{1}{3}}$
Present work	Cellulose (bee-hive)	$\Delta P[Pa] = 0.045\left(\frac{t_{a,in}}{t_{a,\mathrm{Ref}}}\right)^{0.516}\left(\frac{t_w}{t_{w,\mathrm{Ref}}}\right)^{-0.695}\left(\frac{\dot{m}_w}{\dot{m}_{w,\mathrm{Ref}}}\right)^{0.228}\left(\frac{\delta}{\delta_{\mathrm{Ref}}}\right)^{0.626}\mathrm{Re}^{1.044}\,\mathrm{Pr}^{0.33}$
		$Nu = 0.112\left(\frac{t_{a,in}}{t_{a,\mathrm{Ref}}}\right)^{0.9}\left(\frac{t_w}{t_{w,\mathrm{Ref}}}\right)^{-1.487}\left(\frac{\dot{m}_w}{\dot{m}_{w,\mathrm{Ref}}}\right)^{0.186}\left(\frac{\delta}{\delta_{\mathrm{Ref}}}\right)^{-0.48}\mathrm{Re}^{0.527}\,\mathrm{Pr}^{0.33}$
		$Sh = 0.097\left(\frac{t_{a,in}}{t_{a,\mathrm{Ref}}}\right)^{1.374}\left(\frac{t_w}{t_{w,\mathrm{Ref}}}\right)^{4.34}\left(\frac{\dot{m}_w}{\dot{m}_{w,\mathrm{Ref}}}\right)^{0.304}\left(\frac{\delta}{\delta_{\mathrm{Ref}}}\right)^{-0.474}\mathrm{Re}^{0.922}\,Sc^{0.33}$

difference of water vapour in the air. Therefore, the trends of heat and mass transfer coefficients are attained based on the relations between Q_c & ΔT and $\dot{m}_{w,evap}$& $\Delta\rho_v$, respectively as discussed in the previous sections. The highest h_c and h_m can be found are 45 W m^{-2} °C and 0.23 m s^{-1}, respectively as shown in Fig. 8-a and 9-c. Where, h_c and *Nu* enhance by 92.1 and 81%, respectively with decreasing δ from 140 mm to 35 mm at $Re = 1091$ (see Fig. 8-a). Also, h_m and *Sh* improve by 456% and 425% with the increase of water temperature from 25.0 °C to 40.0 °C at $Re = 1091$ (see Fig. 9-c).

The trends of the variation of the heat and mass transfer coefficient with the operating and geometric parameters agree with the trends of the other cooling medium obtained by other investigators [25,40–42]. A quantitate comparison that is given in section 6 shows that the heat and mass transfer coefficient obtained for the current proposed cooling medium (bee-hive cellulose paper) are higher than those of the other medium used in the previous investigations [25,40–42].

5. Experimental correlations

The experimental data and results are regressed to obtain new experimental correlations for the thermal-hydraulic performance parameters (t_{out}, RH_{out}, ΔP, ε_{hum}, $\dot{m}_{w,evap}$, $\dot{Q}_c$, SCC, COP, SWC, *Nu* and *Sh*) of the evaporative cooler in terms of the operating conditions and geometrical design parameters for the proposed cooling pad material. The obtained correlations with their error ranges are illustrated in Table 4. The presented correlations are valid in the ranges that given in Table 2, and the reference values of $t_{a,Ref}$, $t_{w,Ref}$, $\dot{m}_{w,Ref}$and δ_{Ref} are 50 °C, 40 °C, 0.1667 kg/s and 140 mm, respectively. The predictions of these empirical correlations are depicted in Fig. 10.

6. Comparison of present results with literature

The thermal–hydraulic performance of the present direct

evaporative cooler represented by ΔP, ε_{hum}, $\dot{m}_{w,evap}$, *COP*, h_c and h_m are compared with previous data obtained for different selected pad materials in the literature as tabulated in Table 5. The comparison study is carried out with works that have closest operating conditions with the current work to show the prevailing of using the current pad.

As can be seen, the maximum humidifier effectiveness, ε_{hum} can be obtained for the current pad is 0.85, where the pad gives lower pressure drop, ΔP (8 Pa). The maximum$\dot{m}_{w,evap}$, COP, h_c and h_m that can be obtained by the current evaporative pad are 0.9 L min^{-1}, 170, 45 W/m^2 °C and 0.23 m s^{-1}, respectively as compared with all other pad types (see Table 5). Therefore, the current pad material has higher thermal-hydraulic performance rather than existing pad materials within the studied parameters ranges which makes cellulose paper, bee-hive more reliable and applicable as a cooling pad material.

Additionally, comparisons between the current empirical correlations for ΔP, *Nu*, *Sh* with previously available empirical correlations are presented and tabulated in Table 6 in order to proof and validate of using the predicted correlations of the current cooling pad material (cellulose, bee-hive structure) in the ranges of the studied parameters. Firstly, Dowdy and Karabash [40] were presented a simple correlation for *Nu* in terms of pad thickness, *Re* and Pr using cellulous pad cooling material. After that, Liao and Chiu [41] used two typed of cooling pad materials (Coarse & fine fabric PVC sponge mesh) and they offered modified correlations for *Nu* & *Sh* in terms of pad thickness, *Re* and Pr. Lastly, He et al. [42] predicted general empirical correlations for ΔP, *Nu* using three types of cooling pad (cellhouse, PVC, combined), the correlation were correlated in terms of pad thickness, air and water temperatures, *Re* and Pr. In the present work, more general eleven performance parameters correlations were predicted for t_{out}, RH_{out}, ΔP, ε_{hum}, $\dot{m}_{w,evap}$, $\dot{Q}_c$, SCC, COP, SWC, *Nu* and *Sh* using new cooling pad material (cellulose, bee-hive structure) in terms of pad thickness, air and water temperatures, water flow rate, *Re* and Pr to cover more studied parameters than others and hence enlarge the scope of applications. Thus, the difference between the present correlations and previous ones favors of using them and ensure the novelty of the present work.

7. Conclusion

The thermal-hydraulic performance of a new evaporative cooling pad material (cellulose paper, bee-hive structure) is experimentally investigated. The influences of the operating conditions and geometrical parameters on the performance parameters were studied and evaluated. Experimental correlations in dimensionless form for the thermal-hydraulic performance parameters (t_{out}, RH_{out}, ΔP, ε_{hum}, $\dot{m}_{w,evap}$, $\dot{Q}_c$, *SCC*, *COP*, *SWC*, h_c, h_m, *Nu* and *Sh*) of the evaporative cooler pad material in terms of all studied operating and geometrical design parameters are predicted and presented within acceptable error. The most important conclusions of the present study are summarized below:

- Increasing of outlet air temperature, evaporated water rate, cooling capacity, and SWC and decreasing of air relative humidity, humidifier effectiveness, SCC with increasing air velocity were obtained.
- Enhancing humidifier effectiveness and evaporated water rate with increasing pad thickness, air temperature, water temperature and water flow rate.
- Improving COP and cooling capacity with rising air temperature and pad thickness.
- Enhancing heat and mass transfer coefficients, *Nu* and *Sh* numbers with rising the air inlet temperature and humidifier water flow rate and with decreasing the pad thickness. h_c and *Nu* enhance with decreasing δ. Also h_m and *Sh* improve with the increase of the water temperature.
- The highest ε_{hum} and $\dot{m}_{w,evap}$ can be attained are 0.85 & 6.5 g s^{-1}, respectively at 140 mm pad thickness and the highest values of $Q\cdot_c$ and *SCC* are 6.3 kW and 0.6 kWh.kg^{-1}.
- The coefficient of performance increases by raising the frontal air velocity up to 2.2 m s^{-1} and then it decreases with increasing frontal air velocity.

CRediT author statement

S. A. Nada: Conceptualization, Writing- Reviewing and Editing. H. F. Elattar: Investigation, Data curation, M.A. Mahoud: Conducting Experiments, A. Fouda: Writing- Original draft preparation.

Declaration of competing interest

The authors declare that they have no known competing financial interests or personal relationships that could have appeared to influence the work reported in this paper.

References

[1] Abdullah Al-Shaalan M. EER improvement for room Air-conditioners in Saudi arabia. Energy Power Eng 2012;4:439–46.
[2] Nada SA, Said MA. Performance and energy consumptions of split type air conditioning units for different arrangements of outdoor units in confined building shafts. Appl Therm Eng 2017;123:874–90.
[3] Cerci YA. New ideal evaporative freezing cycle. Int J Heat Mass Tran 2003;46:2967–74.
[4] Bishoy Deepak, Sudhakar K. Experimental performance of a direct evaporative cooler in composite climate of India. Energy Build 2017;153:190–200.
[5] Costelloe B, Finn D. Thermal effectiveness characteristics of low approach indirect evaporative cooling systems in buildings. Energy Build 2007;39:1235–43.
[6] Goshayshi HR, Missenden JF, Tozer R. Cooling tower-an energy conservation resource. Applied Thermal Engineering19; 1999. p. 1223–35.
[7] Maheshwari GP, Al-Ragom F, Suri RK. Energy saving potential of an indirect evaporative cooler. Appl Energy 2001;69:69–76.
[8] Sethi VP, Sharma SK. Survey of cooling technologies for worldwide agricultural greenhouse applications. Sol Energy 2007;81:1447–59.
[9] Xu J, Li Y, Wang RZ, Liu W, Zhou P. Experimental performance of evaporative cooling pad systems in greenhouses in humid subtropical climates. Appl Energy 2015;138:291–301.
[10] Guan Lisa, Bennett Michael, Bell John. Evaluating the potential use of direct evaporative cooling in Australia. Energy Build 2015;108:185–94.
[11] Ali Sohani, Sayyaadi Hoseyn. Design and retrofit optimization of the cellulose evaporative cooling pad systems at diverse climatic conditions. Appl Therm Eng 2017;123:1396–418.
[12] Ali Sohani, Mitra Zabihigivi, Hossein Moradi Mohammad, Sayyaadi Hoseyn, Hasani Balyani Hamidreza. A comprehensive performance investigation of cellulose evaporative cooling pad systems using predictive approaches. Appl Therm Eng 2017;110:1589–608.
[13] Al-Badri Alaa Ruhma, Al-Waaly Ahmed AY. The influence of chilled water on the performance of direct evaporative cooling. Energy Build 2017;155:143–50.
[14] Somwanshi Aneesh, Sarkar Niladri. Design and analysis of a hybrid air and water cooler, Engineering Science and Technology. Int J 2020;23(1):101–13.
[15] Tewari Priyam, Mathur Sanjay, Mathur Jyotirmay, Loftness Vivian, Abdul-Aziz Azizan. Advancing building bioclimatic design charts for the use of evaporative cooling in the composite climate of Indi. Energy Build 2019;184:177–92.
[16] Tewari Priyam, Mathur Sanjay, Mathur Jyotirmay. Thermal performance prediction of office buildings using direct evaporative cooling systems in the composite climate of India. Build Environ 2019;157:64–78.
[17] Hao Xiaoli, Zhu Cangzhou, Lin Yaolin, Wang Haiqiao, Zhang Guoqiang, Chen Youming. Optimizing the pad thickness of evaporative air-cooled chiller for maximum energy saving. Energy Build 2013;61:146–52.
[18] Martínez P, Ruiz J, Cutillas CG, Martínez PJ, Kaiser AS, Lucas M. Experimental study on energy performance of a split air-conditioner by using variable thickness evaporative cooling pads coupled to the condenser. Appl Therm Eng 2016;105:1041–50.

[19] Fouda A, Nada SA, Elattar HF. An integrated A/C and HDH water desalination system assisted by solar energy: transient analysis and economical study. Appl Therm Eng 2016;108:1320–35.
[20] Elattar HF, Fouda A, Nada SA. Performance investigation of a novel solar hybrid air conditioning and humidification–dehumidification water desalination system. Desalination 2016;382:28–42.
[21] Nada SA, Elattar HF, Fouda A. Performance analysis of proposed hybrid air conditioning and humidification–dehumidification systems for energy saving and water production in hot and dry climatic regions. Energy Convers Manag 2015;96:208–27.
[22] Nada SA, Elattar HF, Fouda A. Experimental study for hybrid humidification–dehumidification water desalination and air conditioning system. Desalination 2015;363:112–25.
[23] Nada SA, Elattar HF, Fouda A. Energy-efficient hybrid A/C and freshwater production system proposed for high latent load spaces. Int J Energy Res 2019;43(13):6812–26.
[24] Malli Abdollah, Reza Seyf Hamid, Layeghi Mohammad, Sharifian Seyedmehdi, Hamid Behravesh. Investigating the performance of cellulosic evaporative cooling pads. Energy Convers Manag 2011;52:2598–603.
[25] Jain JK, Hindoliya DA. Experimental performance of new evaporative cooling pad materials. Sustainable Cities and Society 2011;1:252–6.
[26] K. Sellami, M. Feddaoui, N. Labsi, M. Najim, M. Oubella,Y.K. Benkahla, Direct evaporative cooling performance of ambientair using a ceramic wet porous layer, Chem Eng Res Des 1 4 2 (2 0 1 9) 225–236.
[27] Laknizi Azzeddine, Mahdaoui Mustapha, Ben Abdellah Abdelatif, Kamal Anoune, Mohamed Bakhouya, Hassan Ezbakhe. Performance analysis and optimal parameters of a direct evaporative pad cooling system under the climate conditions of Morocco. Case Studies in Thermal Engineering 2019;13:100362.
[28] Pervin Abohorlu Doğramacı, Riffat Saffa, Gan Guohui, Aydın Devrim. Experimental study of the potential of eucalyptus fibres for evaporative cooling. Renew Energy 2019;131:250–60.
[29] Nada SA, Fouda A, Mahmoud MA, Elattar HF. Experimental investigation of energy and exergy performance of a direct evaporative cooler using a new pad type. Energy and Buildings; 2019. p. 109449.
[30] Rui Camargo Jose, Daniel Ebinuma Carlos, Luz Silveira José. Experimental performance of a direct evaporative cooler operating during summer in a Brazilian city. Int J Refrig 2005;28:1124–32.
[31] Wu JM, Huang X, Zhang H. Theoretical analysis on heat and mass transfer in a direct evaporative cooler. Appl Therm Eng 2009;29(5–6):980–4.
[32] Wu JM, Huang X, Zhang H. Numerical investigation on the heat and mass transfer in a direct evaporative cooler. Appl Therm Eng 2009;29(1):195–201.
[33] Fouda A, Melikyan Z. A simplified model for analysis of heat and mass transfer in a direct evaporative cooler. Appl Therm Eng 2011;31:932–6.
[34] Kovačević Igor, Sourbron Maarten. The numerical model for direct evaporative cooler. Appl Therm Eng 2017;113:8–19.
[35] Narayan GP, Sharqawy MH, Lienhard V JH, Zubair SM. Thermodynamic analysis of humidification dehumanization desalination cycles. Desalin. Water Treat. 2010;16:339–53.
[36] Sharqawy MH, Antar MA, Zubair SM, Elbashir AM. Optimum thermal design of humidification-dehumidification desalination systems. Desalination 2014;349:10–21.
[37] Moffat RJ. Describing the uncertainties in experimental results. Exp Therm Fluid Sci 1988;1(1):3–17.
[38] Taylor JR. An introduction to error analysis: the study of uncertainties in physical measurements. second ed. Sausalito, CA: University Science Books; 1997.
[39] Koca RW, Hughes WC, Christianson LL. Evaporative cooling pads: test procedure and evaluation. Appl Eng Agric 1991;7(4):485–90.
[40] Dowdy JA, Karabash NS. Experimental determination of heat and mass transfer coefficients in rigid impregnated cellulose evaporative media. Build Eng 1987;93(2):382–95.
[41] Liao CM, Chiu KH. Wind tunnel modeling the system performance of alternative evaporative cooling pads in Taiwan region. Build Environ 2002;37(2):177–87.
[42] He S, Guan Z, Gurgenci H, Hooman K, Lu Y, Alkhedhair AM. Experimental study of film media used for evaporative pre-cooling of air. Energy Convers Manag 2014;87:874–84.